International Journal of Fracture **66:** 295–312, 1994.

The evolution of 'cone' cracks under axi-symmetric loading conditions

DEREK HULL*
Department of Materials Science and Engineering, University of Liverpool, U.K.

Received 11 November 1993; accepted in final form 16 March 1994

Abstract. Cone fractures have been produced in epoxy resin samples in four different test configurations using a cylindrical indenter. The shapes of the cracks were determined using optical microscope focusing methods and it was found that they were strongly dependent on test geometry. Large changes in cone angle with crack length were observed. The evolution of the cracks was determined by mapping the fine river line markings on the fracture surface. In all cases crack nucleation occurred at point sources close to the edge of the indenter and then the crack grew in the material round the base of the indenter before expanding outwards. Numerous crack arrest markings were also mapped. It was found that the number and distribution of crack arrests was dependent on the test configuration and re-nucleation occurred after each arrest. The results are interpreted in terms of the no-twist growth constraint, which applies to crack growth in brittle solids. This leads to characteristic patterns on the fracture surface. It is shown that point nucleation results in a strongly non-symmetric fracture path and that the requirement that nucleation occurs at a point has a significant effect on the interpretation of fracture data in other test configurations.

1. Introduction

Cone cracks are associated with the work of Hertz [1] who provided the solution for the elastic stress fields generated between curved glass surfaces. A detailed review of work on Hertzian cone cracks is given by Lawn [2]. The cone crack produced by a spherical indenter on a planar surface has a characteristic shape and cone angle $\phi = \pi/2 - \alpha$, as illustrated in Fig. 1. It is usually assumed that the cone crack initiates from a favourably oriented flaw close to the contact zone of the indenter. A ring crack then grows round the indenter before growth of the cone crack into the body of the material.

The cone angle depends on the elastic properties of the material, particularly Poisson's ratio ν, and on the conditions of loading. Sub-surface indentation and impulsive loading are included with the Hertzian system in a review of experimental observations by Bahat and Sharpe [3]. They show that for a range of test methods and materials α varies from about 35° to 10° as ν varies from 0.15 to 0.40. The data is broadly consistent with predictions of the influence of ν on the principal stress trajectories by Finnie and Vaidyanathan [4]. There is also evidence from experimental work on the indentation of surfaces with spherical indenters, see for example [5], that α varies with speed of impact.

In describing Hertzian cone cracks it is usually assumed that α is independent of crack length, apart from the region in which the initial ring crack forms. This is consistent with direct observations of cracks formed in conventional Hertz loading conditions and with the predictions of stress analysis. In this paper we consider a family of axi-symmetric cracks in which α varies with crack length. The surfaces have rotational symmetry and may be generated, therefore, by the rotation of a plane curve about an axis in the plane, i.e. they are

* Emeritus Goldsmiths' Professor of Metallurgy, University of Cambridge, U.K.

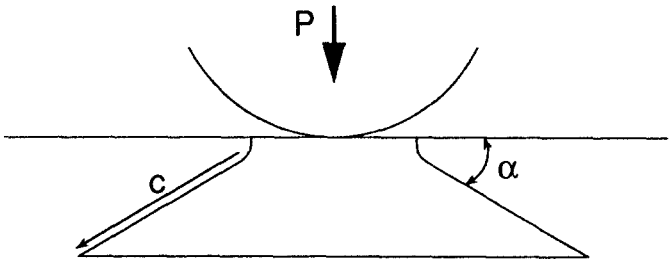

Fig. 1. Cross-section of Hertian cone fracture produced by indentation of a flat surface by a rigid sphere (after Lawn [2]).

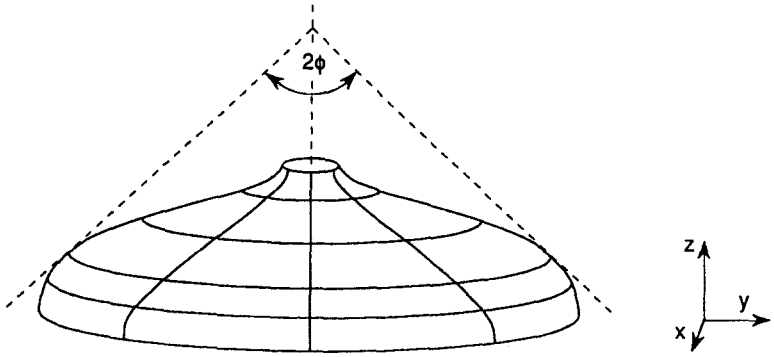

Fig. 2. Surface of revolution showing two orthogonal sets of lines of curvature and an osculating cone.

surfaces of revolution, see Fig. 2. The tangent at any point on the curve then generates an osculating cone with the apex on the axis and an included angle 2ϕ. All the fracture surfaces discussed here have a region which corresponds to the straight-sided cone of Hertzian fracture before developing into more general forms. For convenience and brevity we will refer to all these as cone cracks.

The geometrical rules which govern the evolution of cracks on smoothly curving surfaces have been described elsewhere [6]. Specifically, in the fracture of homogeneous, isotropic, brittle, glassy solids, movement of a crack front on a smoothly curving surface is governed by the requirement that only tilting can occur. The rule applies to each elementary length of the crack tip. This geometrical requirement leads to the conclusion that the instantaneous positions of the crack front on a smoothly curving fracture surface are mapped by the positions of the *lines of curvature* on that surface. On such a surface there are two orthogonal sets of lines of curvature which uniquely map the positions of the crack front and the directions of crack growth for a crack propagating without twist. In the case of a cone, and more general surfaces of revolution, the lines of curvature lie along the latitude and meridional lines, as illustrated in Fig. 2.

Particular attention is given in this paper to the shape of cone-shaped cracks generated in a brittle epoxy resin. The cracks were formed at relatively low stress intensities, because of the ease of crack nucleation, so that the fracture surfaces are very smooth. Fine fractographic details, often masked by more complex features associated with crack growth at high stress intensities, have been used to analyse the evolution of the crack. The instantaneous orientation of the crack front and the direction of crack growth at all positions on the fracture surface have been determined.

Measurements of crack positions and growth directions described in this paper are based on the following properties of a growing crack (we note that a full interpretation of these terms needs further justification, which is outside the scope of the present paper):

1. The orientation of the crack front at any point on the fracture surface determines the alignment of the fine scale characteristic fracture patterns (CFP) which can be observed, at a sufficient magnification, even on very brittle fracture surfaces.
2. The crack front is normal to river line steps and the long dimension of the CFP.
3. The instantaneous position of the crack front coincides with the position of crack arrest or hesitation markings on the fracture surface.
4. The intensity of the CFP and the density of river line steps increases with stress intensity so that it is possible to obtain a qualitative picture of the change in stress intensity during crack growth.
5. The CFP and river line steps are unaffected when crack tilting occurs (see [6] for a detailed definition). River lines remain continuous on smoothly tilting cracks.
6. When a crack grows in a stress field with a mode III component the river line steps develop a quite distinct pattern.

Examples of these fractographic features in epoxy resins have been reviewed and presented in numerous papers, see for example Purslow [7], Robertson and Mindroiu [8] and Young [9].

Experimental results on two aspects of crack surface topology are presented in this paper. First, the effect of loading conditions on the shape and evolution of cone cracks under axi-symmetric loading. Second, the development of a crack on a curved surface when it has been nucleated at a point source.

2. Materials and experiments

2.1. Materials

A Ciba Geigy Araldite LY1927 epoxy resin was used in all the experiments. This is a cold curing low viscosity bismaleidmide resin which was mixed with hardener Araldite HY1927 in proportions 100 : 36 by weight. After pouring into the mould the resin was cured at 20°C for 24 h and post-cured at 100°C for 4 h. Rods of resin 10 mm in diameter were produced by casting into glass tubes which had been treated with a release agent. Similarly, blocks of resin 15 to 40 mm thick were produced using a flat mould.

The properties of the resin are summarised in Table 1. The resin is relatively brittle, is readily machined, and in the context of the present work has the advantage that it shows no evidence of phase separation even at very high resolutions, so that it can be regarded as homogeneous on the scale of the present experiments.

2.2. Test methods

Four fundamentally different axi-symmetric loading tests were used which are illustrated in schematic form in Fig. 3. This figure includes details of the dimensions of the test specimens.

In test A a 10 mm diameter cylindrical specimen was used. A 2 mm diameter hole was drilled down the centre of the specimen using a conventional drill. A second 2 mm diameter drill, which had been ground and polished to produce a flat square end was then used to produce a square ended hole. A 2 mm diameter cylindrical steel indenter rod with square,

Table 1. Properties of post cured epoxy resin at 20°C

Modulus E, (GPa)	3.1
Poisson's ratio ν	0.40
Tensile strength σ^*, (MPa)	70
Elongation to fracture in tension ε^*, (%)	3.8
Fracture toughness K_{Ic}, (MN $m^{-3/2}$)	0.65
Density, $kgm^{-3} \times 10^3$	1.16

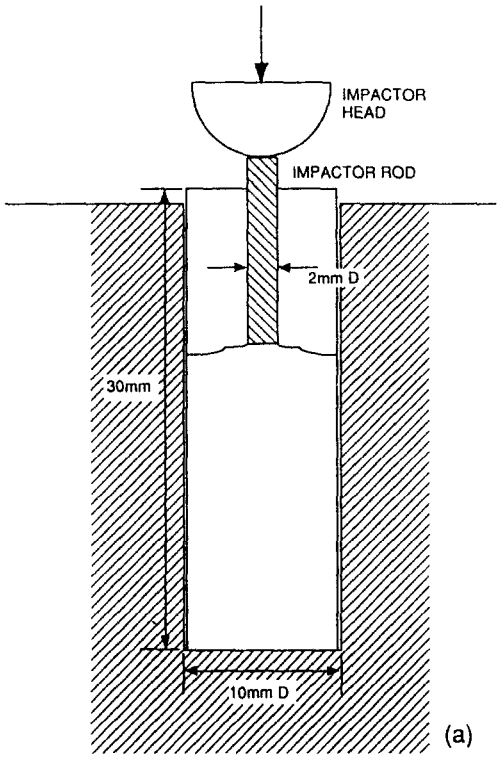

Fig. 3. Four test methods used to generate axi-symmetric cone cracks.

ground and polished, ends was inserted in the hole. The length of the indenter rod was 2 mm greater than the depth of the hole in the test piece. The test piece and the indenter rod were placed in a jig attached to a Zwick pendulum impact machine so that, at the point of impact, the axis of the indenter rod was along the line of motion of the pendulum. The specimen was supported by a solid block of steel. A pendulum with an equivalent mass of 0.464 kg was used to produce impact energies in the range 0 to 2 J. The corresponding velocities at impact were in the range 0 to 2 m/s. Some of the tests were repeated using a conventional drop weight impact facility with a drop weight mass of 0.503 kg. Impact produced a cone crack in the specimen at the end of the indenter rod. After the first impact the indenter rod was removed and a small amount of heavy duty grease was inserted into the hole and the indenter rod re-inserted. A second impact was given to the rod which resulted in the formation and growth of a second cone crack which separated the specimen into two parts.

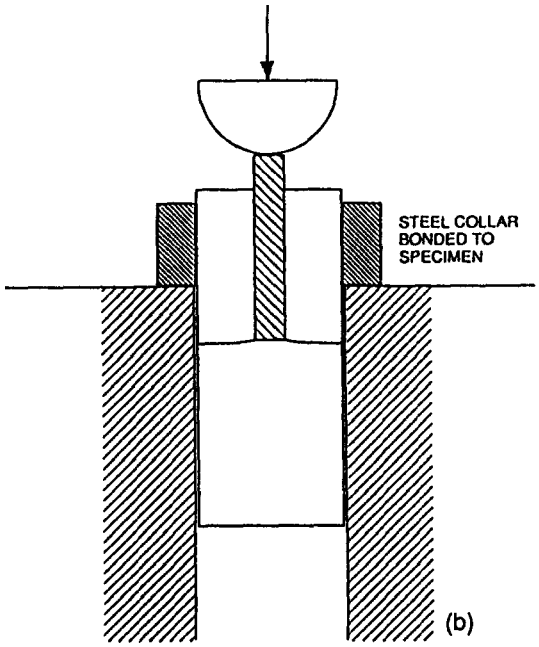

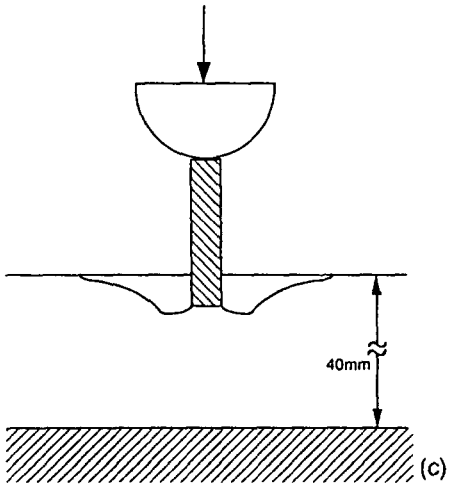

A 10 mm diameter cylindrical specimen was also used for test B. A steel collar was glued to the end of the specimen using an epoxy resin. A square-ended hole was drilled in the centre, as for test A. The specimen was placed in the steel block in the Zwick impact machine. The end of the specimen was not in contact with the block and the steel collar rested against the steel support block as illustrated. At low impact energies a cone crack formed which did not produce complete separation. A second impact was given after grease had been introduced and this resulted in complete separation. At high impact energies complete separation occurred at the first impact.

In test C a parallel sided plate of material 40 mm thick was used. A square-ended hole, typically about 1.5 mm deep, was drilled normal to plane of the block and the indenter rod inserted as before. The block was supported on a solid steel plate and a cone crack was produced by the indenter rod using the drop weight facility. Grease was then introduced into

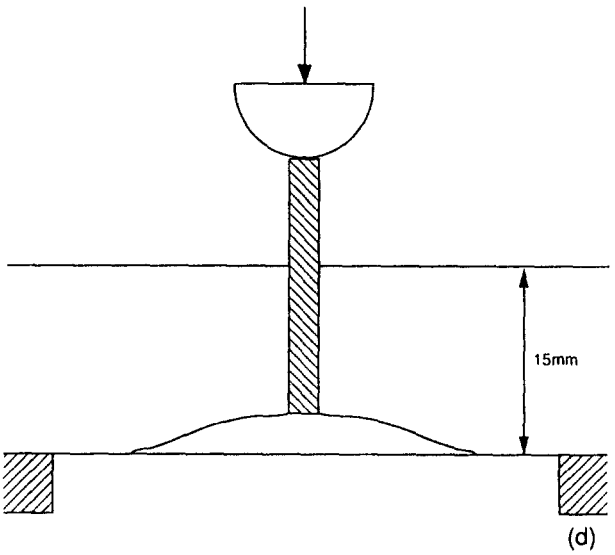

the hole and the impact repeated to produce separation by the formation of a second cone fracture in the opposite sense to the initial cone crack.

The configuration of test D was the same as for test C except that the block of resin, usually about 15 mm thick, was supported on a steel base with a circular hole 30 mm in diameter so that the impact produced a spalling type cone-shaped crack on the lower face of the block. The hole was drilled to about 2 mm from the bottom face of the plate and complete separation occurred at the first impact.

2.3. PROFILE MEASUREMENTS

The shapes of the cone cracks were measured by a focusing method using a Nikon Optiphot microscope fitted with a rectangular mechanical stage, allowing cross travel motion in two orthogonal directions (x and y, see Fig. 2) and measurement of position to within 0.1 mm in each direction. A long working distance 20X objective lens was used with a small depth of focus. As the specimen was moved in the x–y plane the height of the microscope stage was adjusted to keep the surface in focus. The 'height' or z-dimension of the surface was determined to an accuracy of about 0.01 mm using the calibrated fine focus knob on the microscope. The profile along any path was obtained by tracking in the x–y plane using the mechanical stage and recording the x, y and z co-ordinates. The reference surface was taken as the x–y plane which was oriented on the microscope stage normal to the axis of the indenter rod. A typical profile of a radial section is shown in Fig. 4. The points represent individual experimental results and the continuous line is a smoothed curve through the points. In this case test method A was used; the first impact produced a crack, which stopped at the position marked by the arrow, and the second impact, after the introduction of grease, caused complete separation.

A complete contour map of the surface was obtained by determining the x–y co-ordinates of a path on the surface with the z-axis co-ordinate fixed. This was repeated at intervals of 0.1 or 0.2 mm in the z-direction.

A circular graduated stage was used to map out the orientation of the river lines on the fracture surface. Because fracture occurred at relatively low stresses with very small twist

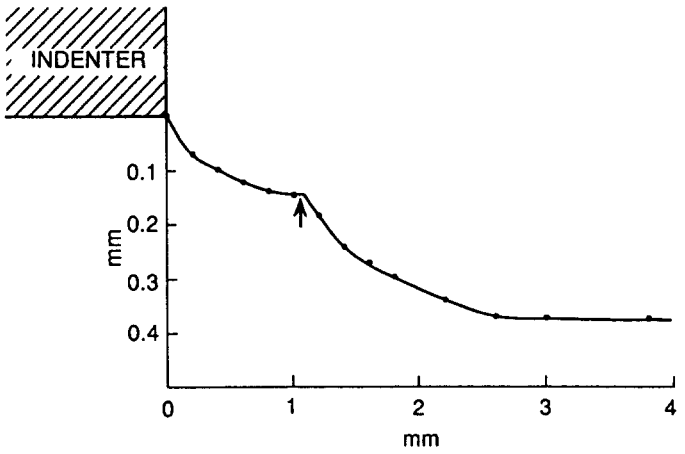

Fig. 4. Typical crack profile showing individual experimental measurements.

forces, particularly in test configuration D, there were only a few river lines and these often extended across the whole surface. Individual lines were tracked across the surface and the co-ordinates in the x–y plane and the orientation of the line were recorded as a projection of the line on the x–y reference surface. A similar method was used to map out the position of the arrest or hesitation markings.

Optical photographs were taken with the Nikon microscope using transmitted light. Some photographs were taken with reflected light after the fracture surfaces had been coated with a thin layer of vapour deposited gold.

3. Effect of test configuration on crack shape

The cracks formed by the four test methods closely approximated to surfaces of revolution with the axis of symmetry parallel to the axis of the impact rod. The fracture surfaces showed circular and radial features. An example is shown in Fig. 5 for a crack produced using test A; the radial markings are river lines and the circular features are hesitation markings. This photographic image is essentially the projection of the surface markings on the 3-D surface of the cone-shaped crack onto the x–y plane. A large depth of focus lens was used to ensure that the majority of the surface was in focus.

Section profiles for cracks produced by all four test methods are illustrated in Fig. 6 (note that, for clarity, the origins in the z-direction have been displaced for tests B, C and D). In Fig. 6a the scale in the z-direction and the radial direction are different. The arrows mark positions of crack arrest and the short vertical lines the positions of hesitation markings. In Fig. 6b the scale of both axes is the same so that the tangent at any point accurately represents the cone angle α at that point. Results from all four test methods are shown on the same diagrams so that direct comparisons can be made. A common feature of all the cracks, independent of test method, was the initial shape of the cone. Subsequent growth of the crack was strongly dependent on the loading mode.

Three curves are shown in Fig. 6 for test method A for different intial impact energies. The length of the crack formed by the initial impact (marked by the arrows in Fig. 6a) increased with impact energy. A full set of results is shown in Fig. 7. No cracks were formed at an impact energy of 0.008 J and at impacts above 0.9 J secondary cracking occurred by the formation of

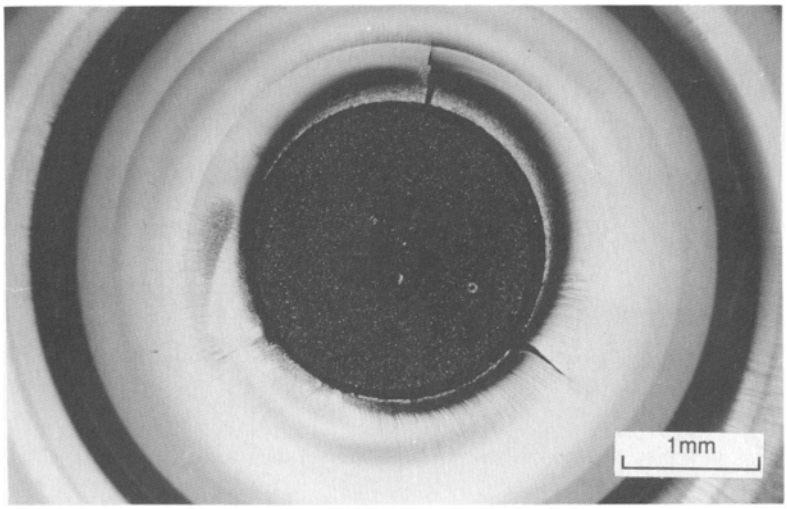

Fig. 5. Optical micrograph of cone crack produced using test method A showing circular hesitation lines and radial river lines.

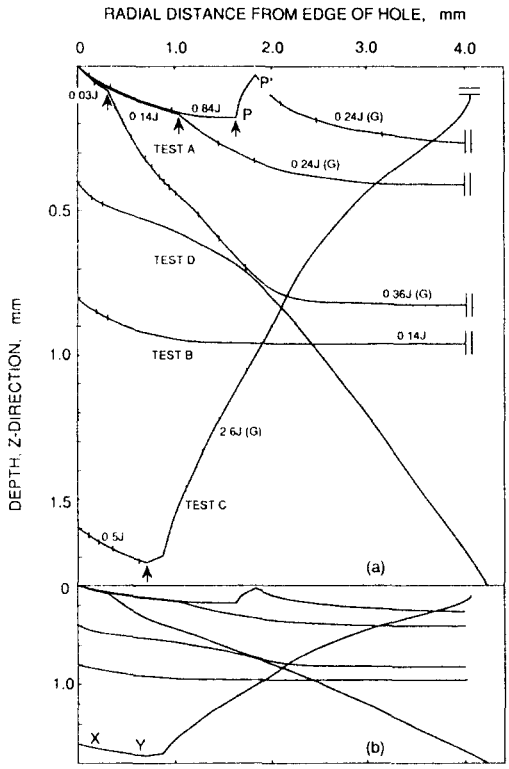

Fig. 6. Crack profiles produced by four test methods, (a) with enlarged z-axis showing position or arrest (arrows) and hesitation markings (short vertical lines), double lines mark the surface of the specimen, (b) with same scale on both axis to give a direct indication of the cone angles; note, the curves have been displaced on the z- axis for clarity and G means grease.

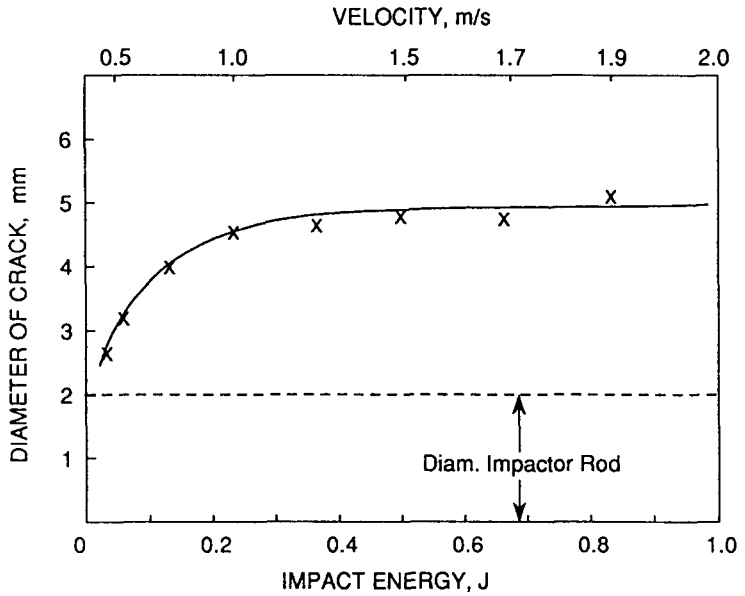

Fig. 7. Effect of impact energy and impact velocity on the projected length of the first cone crack using test method A.

radial-median cracks (see [2]) and general fragmentation at the end of the indenter without any further increase in the length of the primary cone crack. For impact energies above about 0.4 J a second inverted cone crack was formed at the tip of the initial crack (see for example, section P–P' of the crack formed at 0.84 J shown in Fig. 6). The source of the stress field producing this second cone crack is uncertain. Chaudhri and Brophy [10] observed curving crack tips on cone cracks during unloading after high speed impacts. Alternatively, there is the possibility that the second cone is caused by an elastic wave reflected from the bottom of the test specimen. After the introduction of grease and a second impact a new cone crack formed and grew to the boundaries of the specimen causing complete separation. Pressure on the grease from the indenter produced a hydrostatic pressure in the initial cone crack. The boundary between the two cones is defined by an arrest ring. The shape of the grease-generated cone was strongly dependent on the length of the initial cone crack.

The cone cracks produced by test B were much flatter than for test A although the initial shape of the crack was similar. The profile shown in Fig. 6 is for a test sample after an impact of 0.14 J. In test A this impact energy produced a crack about 4 mm in diameter but in test B it was sufficient to cause complete separation of the specimen (10 mm diameter).

In test C a normal cone crack was generated by the first impact. The diameter of the crack depended on the impact energy, as in test A, but for a given impact energy the diameter of the crack was much smaller. Thus, for the example shown in Fig. 6, an impact of 0.5 J produced a crack about 3.4 mm diameter in test C whereas in test A this energy produced a crack about 4.9 mm in diameter. A secondary inverted cone crack was also produced by a 0.5 J impact in test C. After the introduction of grease relatively large impact energies were required to cause separation; this energy was dependent on the depth of the drilled hole. The pressure generated in the grease by the impact resulted in the nucleation of a new cone crack which grew to the free surface and resulted in the formation of an inverted cone-shaped surface.

In test D the initial shape of the cone was similar to the other tests but the subsequent growth was strongly influenced by the presence of the free surface. Low impact energies were

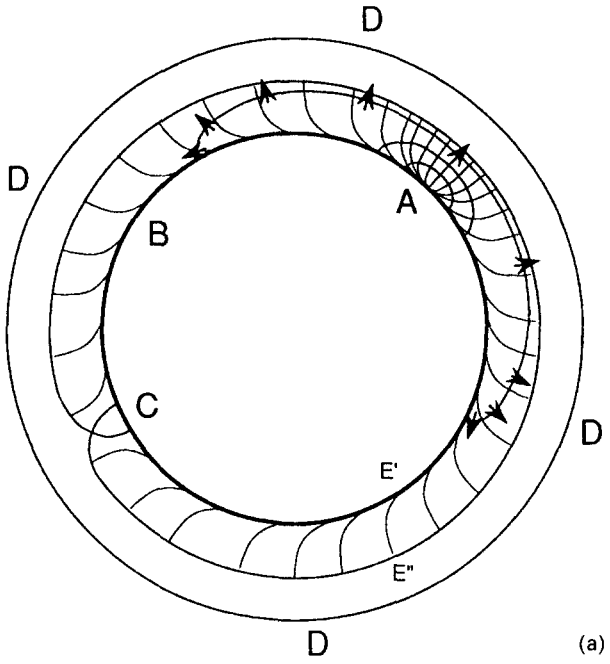

Fig. 8. Experimental observations on evolution of a cone crack at base of indenter produced by test method D, (a) shape and orientation of river lines (fine lines) and predicted position of evolving crack front (thick lines), one such line is marked by arrows showing direction of crack growth, (b) optical micrograph of crack nucleation region A, (c) optical micrograph of region B, (d) optical micrograph of crack overlap region C.

required to cause complete separation; the energy required was dependent on the distance of the bottom of the hole from the free surface.

4. Nucleation and first stages of evolution of cone cracks

Figure 6 shows that the initial shape of the crack is independent of the test procedure. This is not unexpected since the stress field generated by the indenter is almost identical for short cracks. It is only as the stress field is influenced by the dimensions of the test sample, i.e. the presence of free surfaces, and by the external constraints applied to these surfaces, that the cracks develop into shapes which are dependent on the test method. In this section we are concerned with the initial stages of crack nucleation and growth.

The actual details of nucleation varied from one test to the next even when the same test procedure was used. However, the sequence of events was the same and is illustrated by the example in Fig. 8. Figure 8a shows in diagrammatic form the distribution and shape of river lines around the perimeter of the hole in the specimen. The diagram is based on direct observations of the fracture surface. Three optical micrographs of important features are shown in Figs. 8b to 8d. It is important to recognise that the diagram and the photographs are two dimensional representations, in the x-y plane, of a three dimensional surface. Thus, the photographs only have small regions which are in sharp focus. The crack nucleated at a point site (Fig. 8b and point A in Fig. 8a) on the perimeter of the drilled hole. Fine river lines extend from the nucleation site. The instantaneous positions of the expanding crack front were determined by mapping lines normal to the river lines as illustrated by the thicker lines in Fig. 8a. The crack then grew rapidly round the perimeter of the hole in both clockwise

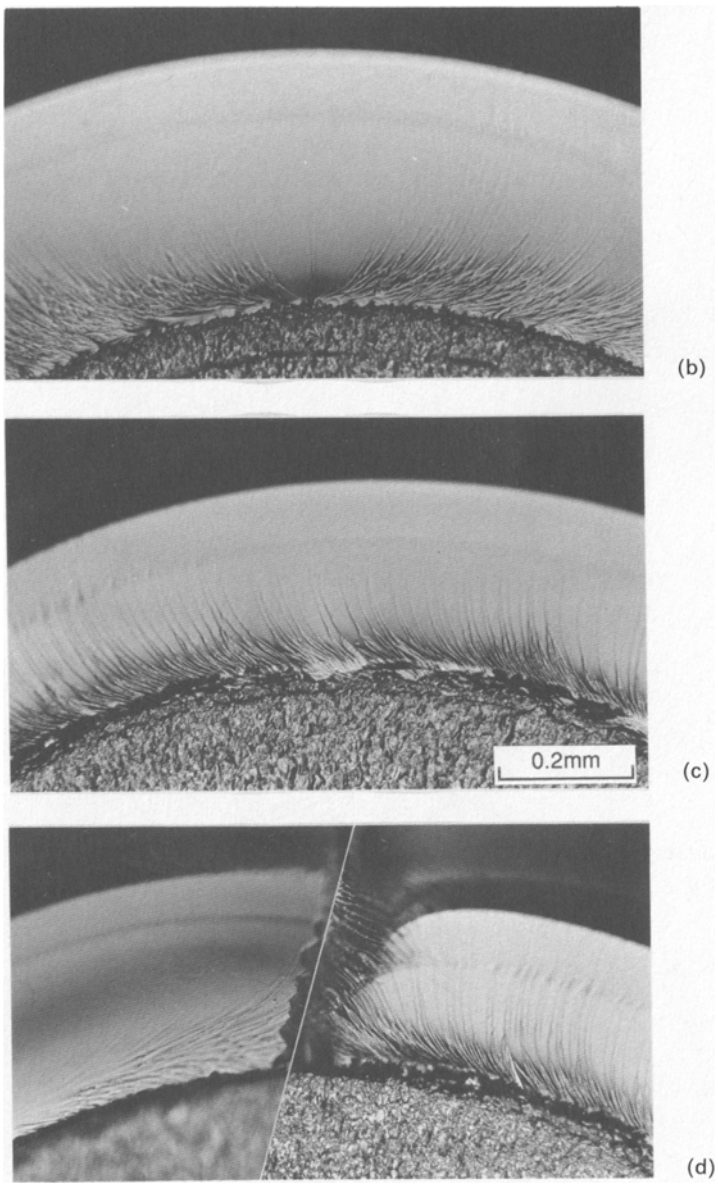

and anti-clockwise directions and comparatively slowly in the orthogonal direction. A typical region (point B in Fig. 8a) is shown in Fig. 8c. When the two crack fronts met (Fig. 8d and point C in Fig. 8a) they were on slightly different surfaces and grew past each other. Eventually they interacted and tilted towards each other forming an isolated sliver of material lying normal to the perimeter of the hole which broke off forming a jagged edge. When the crack had grown completely round the perimeter a circular crack front (D-D-D-D in Fig. 8a) was established which then expanded on a cone-shaped surface.

In many cases, particularly at higher impact energies, more than one crack was nucleated on the perimeter (see for example Fig. 5). Each crack expanded around the perimeter and

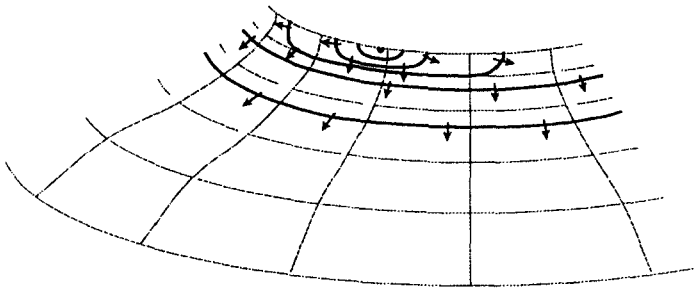

Fig. 9. Perspective view of cone crack showing crack evolving on a smoothly curving surface.

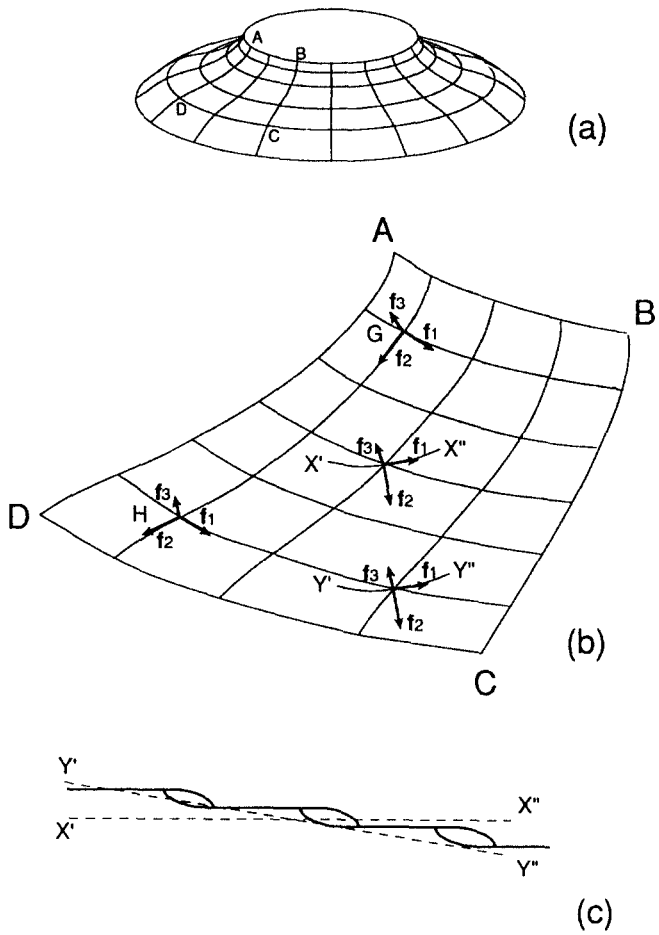

Fig. 10. Lines of curvature on a section of a smoothly curving cone-shaped fracture surface illustrating no-twist growth and twist growth leading to the formation of river lines.

eventually interacted with other cracks as described above. A circular crack front then became established and expanded in the normal way.

A three-dimensional perspective view of the processes illustrated in Fig. 8 is shown in Fig. 9. It is clear that the crack has grown on a curved surface. We have demonstrated previously [6] that there are geometrical restrictions to the growth of cracks in brittle materials because of the condition that only tilting movements at the crack tip are possible. In particular, it

was shown that, for a cone-shaped crack nucleated at a point source, the growth of the crack must occur in a very precise way if twist forces are to be avoided at the crack tip. The main arguments can be understood by reference to Fig. 10. Suppose that the surface represented schematically by ABCD is part of the cone-shaped surface generated by a crack. The fine lines are the lines of curvature on the surface and they represent the mapping of the crack front positions required if twist is to be avoided. More specifically, every point on the crack surface, the orientation of the surface and the crack tip, when the crack passes through that point, is described by a principal frame field of three vectors $\mathbf{f}_1$, $\mathbf{f}_2$ and $\mathbf{f}_3$ with $\mathbf{f}_1$ normal to the crack plane, $\mathbf{f}_2$ parallel to the direction of crack propagation and $\mathbf{f}_3$ tangential to the crack tip. In these terms the condition that the crack grows without twist is that there is no rotation about $\mathbf{f}_2$ moving along the direction of crack propagation. Thus, when a crack at G, represented by the principal frame field illustrated in the diagram, moves along a line of curvature to H there is no rotation of the principal frame field about $\mathbf{f}_2$. It follows that the surface ABCD can be generated without twist by a crack front lying along AB growing to DC providing the crack front is always along a line of curvature. Similarly, the surface ABCD can be generated, in principle, without twist by a crack AD moving to BC. Suppose, hypothetically, that a smooth crack is introduced into the surface with the crack tip lying along X'-X'' and that it moves in the surface ABCD to Y'-Y''. In this case $\mathbf{f}_2$ and $\mathbf{f}_3$ at X and Y do not lie along lines of curvature and there is rotation of the principal frame field about $\mathbf{f}_2$, i.e. twist has occurred. Figure 10c shows a section through the crack tip at X'-X'' and the orientation of the crack tip at Y'-Y'' which has twisted. To avoid twist the crack splits up onto a number of separate surfaces and the steps between these surfaces are sections through river lines.

When these arguments are applied to the movements illustrated in Fig. 8 and 9 it is clear that these no-twist conditions are not satisfied. The curved crack E'-E'' in Fig. 8a is equivalent to X'-X'' in Fig. 10. As the crack spins round the perimeter of the hole on the curved surface twist forces are produced and this results in the river line patterns. In reality the river lines mark out the boundaries of a multitude of overlapping cracks, as illustrated in Fig. 22 of [6], which provide the 'macroscopic twist' by the formation of discrete steps.

5. Expansion of a crack to form cone-shaped surfaces

The circular crack D-D-D-D (Fig. 8a) which forms when the crack has grown completely round the perimeter of the indenter can grow on any surface of revolution without generating twist forces [6] providing the plane containing the crack tip is normal to the axis of revolution, i.e. the crack tip lies along a line of curvature, which in this case is a line of latitude. This is equivalent to the example in Fig. 10b where the crack AB moves to CD. This means that river lines do not form and the surface is very smooth, providing the crack grows at low stress intensities. The isolated river lines shown on the cone surface in Fig. 5 are indicative of small deviations of the crack from the surface of revolution which could result from the crack nucleation event or a slight misalignment of the indenter.

A map of a cone-shaped surface, generated using test method D, is shown in Fig. 11. The z-axis is normal to the map and parallel to the direction of loading. The contour lines of the surface approximate closely to circles except in the region around the indenter where nucleation occurred (point N). Away from the nucleation region the surface was very smooth and only isolated river lines were observed. The position and orientation of some of these lines were measured using the method described in Section 2.3, and then plotted on the contour map in Fig. 11. On an ideal surface of revolution all these lines would radiate from the axis

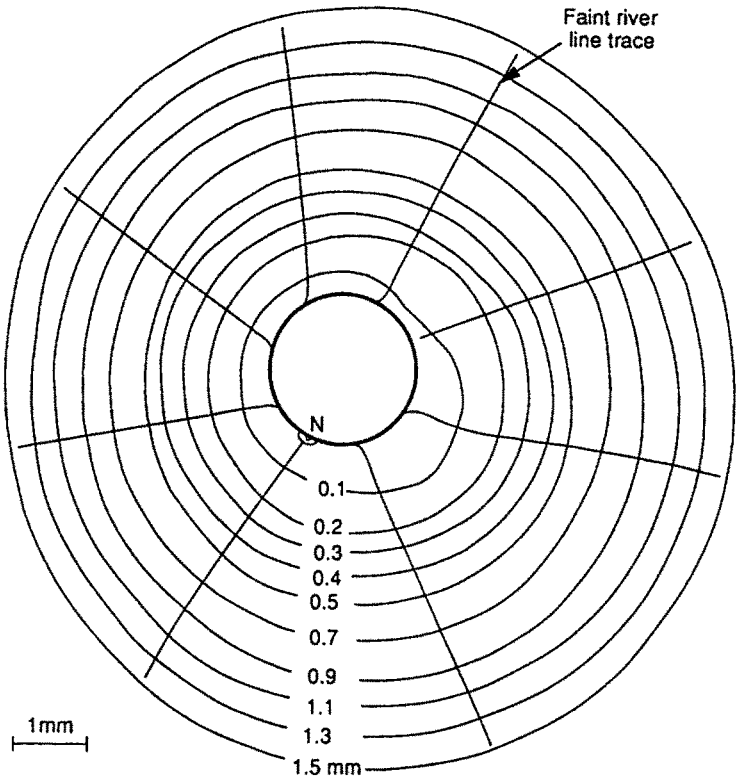

Fig. 11. Experimental observations on the shape of a cone fracture generated by test method D plotted as a contour map with the reference surface (x-y plane) normal to axis of impact, circular lines are contour lines (not lines of curvature) and radial lines map the direction of fine river lines (which follow one set of lines of curvature).

of revolution. In this case there are large deviations in the positions of the experimentally observed lines close to the nucleation region and small deviations elsewhere. Clearly, the nucleation process leads to some non-symmetry which affects subsequent growth of the crack.

An important feature of the growth of the cone-shaped fracture is the formation of hesitation or arrest lines on the fracture surface, i.e. the circular features in Fig. 5, not to be confused with the contour lines in Fig. 11. The occurrence and distribution of these markings was dependent on test methods as illustrated in Fig. 6a. The markings can be divided into two groups. First, markings which are associated unambiguously with cracks which have stopped: marked by an arrow in Fig. 6a. Second, markings which map out the instantaneous positions of the crack front, for which there is no unambiguous evidence that the crack has stopped; marked by short vertical lines in Fig. 6a. In the latter case we assume that the crack has stopped, albeit for a very short time; the fractographic features are basically identical to those of the former although the intensity of markings is less.

If the crack has stopped there will be a redistribution of stress and the path of fracture during subsequent extension will not be the same as for a continuously growing crack. This has two consequences which are evident on the fracture surfaces. First, the angle of crack growth is different so that the crack surface tilts discontinuously at the hesitation line. This is revealed in optical microscopy by a sharp change in the intensity of reflected or transmitted light (see Fig. 12). Second, the crack must renucleate at every hesitation line. Nucleation must occur at

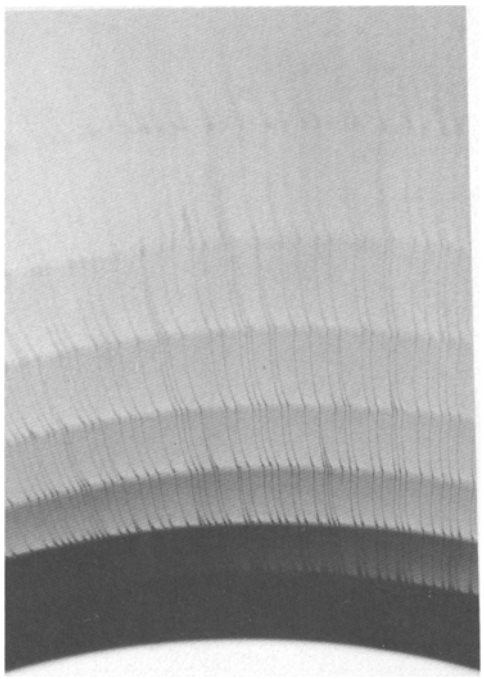

Fig. 12. Optical micrograph showing tilts associated with arrest and hesitation lines in a specimen tested by method A.

a point and then the crack unzips along the original crack front. A set of hesitation markings is shown in Fig. 13. As before the river lines on the surface map out the local directions of crack growth. On one side of the hesitation line the river lines are normal to the hesitation line and on the other side they form curved patterns. This is because the crack renucleates somewhere along CD and then unzips by rapid growth around CD before expanding uniformly towards EF. This process is equivalent to the initial nucleation process described in Section 4. Multiple re-nucleation can occur along the crack front. Figure 14 shows an example in which the unzipping process has occurred in opposite directions at successive hesitation lines.

Figure 6a shows that, in the initial stages of crack growth, hesitation markings occur in all test modes. For test modes A and C hesitation markings occurred at all stages of crack growth. For test modes B and D, in which the initial crack resulted in complete fracture, no hesitation markings were observed except in the initial stages. These different responses can be attributed to the stability of crack growth. Lawn [2] has demonstrated the requirements of crack growth stability for the conventional Hertz test. The conditions in the Hertz test are most closely related to those for the first crack in test mode C, and to a lesser degree, to the initial stages of crack growth in all the test modes used in this work. Under conditions of stable growth the stick-slip effect is important in materials in which the stress intensity to initiate crack growth is greater than that required for growth. In effect the excess energy associated with nucleation results in rapid crack growth followed by stress relaxation which leads to the crack stopping momentarily, hence the formation of the hesitation lines. The distributions of hesitation lines in Fig. 6a give an insight into the stability of crack growth in the different test modes.

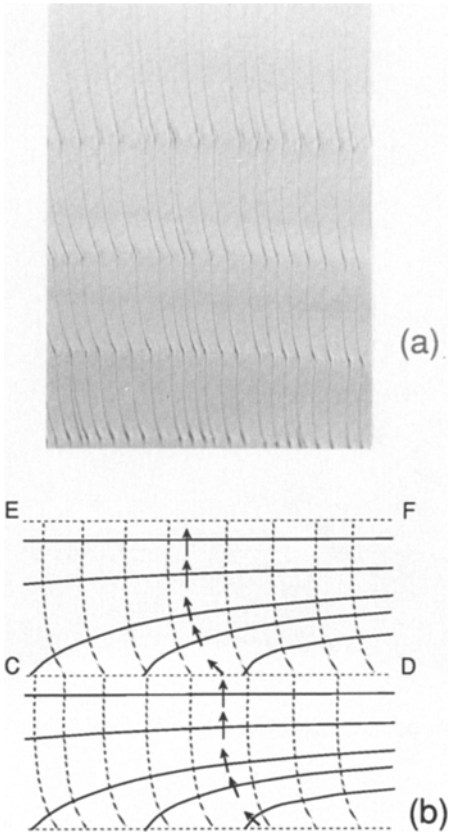

Fig. 13. (a) Optical micrograph, and (b) schematic, of hesitation lines and associated river lines showing the evolution of crack by unzipping.

6. Discussion and conclusions

The emphasis in this paper is on the shape of cracks and the inter-relation between test conditions and crack evolution at a macro and a micro scale. Each of the test modes used could be the subject of a detailed theoretical analysis to determine the stress fields and hence predict the path of fracture on the basis of some fracture mechanics criterion. The prospect is a daunting one because of the inherent complexity, particularly if stress relaxation associated with the growing crack and other dynamic effects are taken into account. Relaxation effects are clearly important when the cracks stop as discussed in the previous section. The re-nucleation processes associated with each crack stopping event mean that the path of fracture is no longer on a continuous smoothly curving surface; local twist forces are created and these lead to the river line markings.

Only a brief mention has been made to the effects of stress intensity on the fracture surface appearance. It is well known that the roughness of fracture surfaces increases with increasing K_I as typified, for example, by the observation of mirror, mist and hackle regions on the surface of fractured tensile specimens. If the stress to nucleate fracture is high then the initial K_I is high and a rough fracture surface is generated almost immediately. In the present experiments the cone-shaped cracks were nucleated at very low K_I values because the drilling process, to

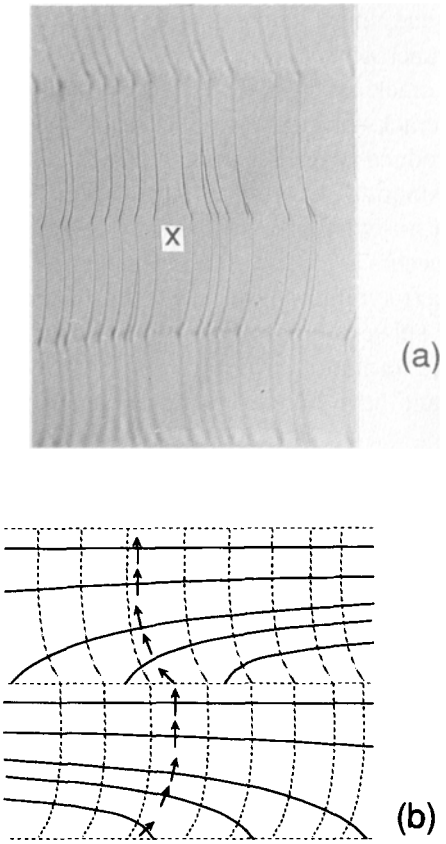

Fig. 14. (a) Optical micrograph, and (b) schematic, of hesitation lines and associated river lines showing the evolution of crack by unzipping in opposite directions: note, at point X cracks unzipping in opposite directions meet.

produce the hole for the indenter rod, produced a large number of incipient cracks around the perimeter of the hole.

Some of the experiments reported here were inspired by the work of Bahat and Sharpe [3] who were particularly interested in the effect of Poisson's ratio on the cone angle α. However, the present work indicates that the concept of a constant α for cone cracks needs careful definition. Hertz cone cracks, for which a constant α is observed and predicted, are generated in semi-infinite solids. When the dimensions and geometry of the specimen influence the stress fields the concept of a constant α must be abandoned. Close to the indenter the stress field will approximate to the semi-infinite case. In the present work, the initial growth of the cone after the nucleation stage is approximately linear, as shown in region X-Y in Fig. 6b, and the value of α is about 7 to 10° in general agreement with the values predicted for a material with $\nu = 0.40$.

The introduction of grease, particularly in test methods A and D, resulted in completely different fracture paths owing to the hydrostatic pressure generated by the impacted grease. The cracks produced under hydraulic pressure showed hesitation markings presumably caused by the stability of crack growth and the hydrodynamic characteristics of the grease. No attempt has been made to evaluate these effects.

The most important issue, in the context of the evolution of fracture surfaces, concerns the inter-relation of the macroscopic stress fields and the local stress fields resulting from the requirement that the crack must nucleate a point source. This appears to be the case even for the very sharp cracks associated with hesitation lines. In all these tests the axi-symmetric loading will produce an axi-symmetric principal stress field. The predicted path of fracture will then lie on a smoothly curving surface on which the lines of curvature satisfy the requirements for a perfect no-twisting cone-shaped fracture path. However, the requirement that the crack nucleation occurs at a point source changes all this. Even though the externally applied load is perfectly axi-symmetric, once a crack has nucleated the stress fields are no longer axi-symmetric and subsequent growth of the crack cannot occur without twist forces being generated. Hence the formation of river lines. These considerations apply to nearly all brittle fracture situations and have important consequences for the interpretation of fracture experiments.

Acknowledgements

My thanks to Elizabeth Yoffe of Cambridge University for her interest and willingness to listen and to Professor Peter Goodhew of Liverpool University for allowing me to work in his Department.

References

1. H.H. Hertz, *Hertz's Miscellaneous Papers*, Macmillan, London (1896).
2. B.R. Lawn, *Fracture of Brittle Solids*, 2nd edn., Cambridge University Press, Cambridge (1993).
3. D. Bahat and M.R. Sharpe, *Journal of Materials Science* 17 (1982) 1167–1170.
4. I. Finnie and S. Vaidyanathan, in *Fracture Mechanics of Ceramics*, Vol. 1, R.C. Bradt, D.P.H. Hasselman and F.F. Lange (eds.), Plenum Press (1974) 231–244.
5. M.M. Chaudhri and C.R. Kurkjian, *Journal of the American Ceramic Society* 69 (1986) 404–410.
6. D. Hull, *International Journal of Fracture* 62 (1993) 119–138.
7. D. Purslow, *Composites* 17 (1986) 289–303.
8. R.E. Robertson and V.E. Mindroiu, *Polymer Engineering and Science* 27 (1987) 55–61.
9. R.J. Young, in *Developments in Reinforced Plastics -1*, G. Pritchard (ed.), Applied Science Publishers (1980) 257–283.
10. M.M. Chaudhri and P.A. Brophy, *Journal of Materials Science* 15 (1980) 345–352.